



The chloroplast RNA-binding protein CP29A supports *rbcL* expression during cold acclimation

Benjamin Lenzen^{a,1} , Florian Rösch^{a,1} , Julia Legen^a , Hannes Ruwe^a , Nitin Kachariya^{b,c} , Michael Sattler^{b,c}, Ian Small^d, and Christian Schmitz-Linneweber^{a,2}

Edited by David B. Stern, Boyce Thompson Institute for Plant Research, Ithaca, NY; received February 26, 2024; accepted December 17, 2024 by Editorial Board Member Julia Bailey-Serres

The chloroplast genome encodes key components of the photosynthetic light reaction machinery as well as the large subunit of the enzyme central for carbon fixation, Ribulose-1,5-bisphosphat-carboxylase/-oxygenase (RuBisCo). Its expression is predominantly regulated posttranscriptionally, with nuclear-encoded RNA-binding proteins (RBPs) playing a key role. Mutants of chloroplast gene expression factors often exhibit impaired chloroplast biogenesis, especially in cold conditions. Low temperatures pose a challenge for plants as this leads to electron imbalances and oxidative damage. A well-known response of plants to this problem is to increase the production of RuBisCo and other Calvin Cycle enzymes in the cold, but how this is achieved is unclear. The chloroplast RBP CP29A has been shown to be essential for cold resistance in growing leaf tissue of *Arabidopsis thaliana*. Here, we examined CP29A–RNA interaction sites at nucleotide resolution. We found that CP29A preferentially binds to the 5′-untranslated region of *rbcL*, downstream of the binding site of the pentatricopeptide repeat protein MATURATION OF RBCL 1 (MRL1). MRL1 is an RBP known to be necessary for the accumulation of *rbcL*. In *Arabidopsis* mutants lacking CP29A, we were unable to observe significant effects on *rbcL*, possibly due to CP29A's restricted role in a limited number of cells at the base of leaves. In contrast, CRISPR/Cas9-induced mutants of tobacco NtCP29A exhibit cold-dependent photosynthetic deficiencies throughout the entire leaf blade. This is associated with a parallel reduction in *rbcL* mRNA and RbcL protein accumulation. Our work indicates that a chloroplast RNA-binding protein contributes to cold acclimation of RbcL production.

chloroplast | RNA binding | cold acclimation | RuBisCo | CLIP

The chloroplast is crucial in how plants adapt to cold stress (1). Cold tolerance in many plants relies on photosynthetic acclimation during low-temperature growth. When exposed to light in cold conditions, the Calvin cycle enzyme activity declines, and thus, the availability of electron acceptors becomes limited, while at the same time, the plastoquinone pool is fully reduced. This leads to a buildup of reactive oxygen species, triggering signals that control nuclear gene expression. The chloroplast's response to cold directly affects a plant's ability to withstand low temperatures (1), indicating that its adjustment is crucial for overall resilience to cold.

Chloroplasts undergo intricate adjustments in gene expression to acclimate to cold temperatures, with critical roles played by transcripts encoding key components of photosynthesis such as *rbcL*, encoding the large subunit of RuBisCo. These adjustments involve the action of various regulatory proteins, including MRL1, a pentatricopeptide repeat (PPR) protein known to target the *rbcL* 5′-UTR and to control *rbcL* mRNA levels, by preventing RNA degradation (2). Another factor associated with *rbcL* mRNA is the chloroplast ribonucleoprotein (cpRNP) CP29A (3). Proteins of the cpRNP family are characterized by two RNA recognition motifs (RRM) connected by a linker domain. They exhibit high affinity for U/G homopolymers, but lower affinity for cytosine (C) and no affinity for adenine (A) homopolymers (4). The interaction of cpRNPs with chloroplast RNAs was examined through a series of in vitro and in vivo tests. Intron-lacking transfer RNAs (tRNAs) and ribosomal RNAs (rRNAs) were found to have little or no affinity for cpRNPs (5). In contrast, cpRNPs were found to associate with various mRNAs and some intron-containing tRNAs (3, 5, 6). A highly enriched transcript in IPs of CP29A was *rbcL* (3). Beyond the identification of coprecipitating transcripts, no details on binding sites in vivo nor whether binding of RNA is direct in vivo are known.

Cross-linking followed by immunoprecipitation (CLIP) employs ultraviolet (UV) light to create covalent bonds, preserving direct protein–RNA interactions (7–9). Such non-reversible bonds allow harsh washing conditions thereby reducing false positives and

Significance

This study unveils the role of CP29A, a chloroplast-localized RNA-binding protein, in facilitating plants' acclimation to cold environments. We found that a preferred target of CP29A is the *rbcL* messenger RNA, encoding a subunit of RuBisCO—a key enzyme in photosynthesis and the most abundant protein on Earth. Our study reveals that CP29A is essential for the full accumulation of *rbcL* mRNA and for the accumulation of the *rbcL*-encoded large subunit of Ribulose-1,5-bisphosphat-carboxylase/-oxygenase in response to cold exposure, functioning through its binding to the 5′-untranslated regions (UTRs) of *rbcL*.

Author affiliations: ^aMolecular Genetics, Institute of Biology, Faculty of Life Sciences, Humboldt Universität zu Berlin, Berlin 10115, Germany; ^bMolecular Targets and Therapeutics Center, Helmholtz Munich, Institute of Structural Biology, Neuherberg 85764, Germany; ^cDepartment of Bioscience, Bavarian NMR Center, Technical University Munich School of Natural Sciences, Technical University of Munich, Garching 85747, Germany; and ^dAustralian Research Council Centre of Excellence in Plant Energy Biology, School of Molecular Sciences, The University of Western Australia, Perth, WA 6009, Australia

Author contributions: M.S., I.S., and C.S.-L. designed research; B.L., F.R., J.L., H.R., and N.K. performed research; B.L., F.R., J.L., H.R., and N.K. analyzed data; and M.S., I.S., and C.S.-L. wrote the paper.

The authors declare no competing interest.

This article is a PNAS Direct Submission. D.B.S. is a guest editor invited by the Editorial Board.

Copyright © 2025 the Author(s). Published by PNAS. This article is distributed under [Creative Commons Attribution-NonCommercial-NoDerivatives License 4.0 \(CC BY-NC-ND\)](https://creativecommons.org/licenses/by-nc-nd/4.0/).

¹B.L. and F.R. contributed equally to this work.

²To whom correspondence may be addressed. Email: christian.schmitz-linneweber@rz.hu-berlin.de.

This article contains supporting information online at <https://www.pnas.org/lookup/suppl/doi:10.1073/pnas.2403969122/-/DCSupplemental>.

Published January 29, 2025.

facilitating the identification of specific RNA targets. Another advantage of CLIP-based protocols is the higher resolution and thus the ability to identify target sites rather than target RNAs. As the molecular function of RNA-binding proteins (RBPs) is highly dependent on their binding position within target transcripts, knowledge of binding sites can provide helpful information with respect to an RBP's biological role. Therefore, a CLIP-based approach was established for the investigation of the molecular role of CP29A in organellar gene expression.

Results

Enhanced Cross-Linking and Immunoprecipitation (eCLIP) Demonstrates That CP29A Binds RNA Directly In Vivo and Has a Preference For U-Rich Sequence Elements. Only a few in vivo cross-linking and immunoprecipitation experiments, followed by next-generation sequencing (CLIP-Seq) have been conducted in plants (8, 10, 11), and none in chloroplasts. We adapted the eCLIP protocol (12, 13) for chloroplasts, employing specific antibodies for CP29A and CP33B, another cpRNP family member. The binding pattern of CP33B, revealed through prior RIP-Chip results, differs substantially from CP29A (3, 14, 15). Analyzing two RBPs with different target specificities in parallel can unveil potential bias and false positives in the procedure.

We used 10 billion chloroplasts per CLIP sample, subjecting them to UV cross-linking, followed by lysis and immunoprecipitation with CP29A and CP33B antibodies. Successful precipitation of protein–RNA complexes was confirmed via western blot and radio-labeling of bound RNA (*SI Appendix, Fig. S1 A and B*). The RNA–protein complexes, larger than the ribonucleoprotein by itself, exhibited size variation visible as a smear on the autoradiogram above the respective cpRNP size (*SI Appendix, Fig. S1B*). The corresponding blot section was excised, treated with protease to release RNAs from the nitrocellulose, and the released RNA was processed for library preparation compatible with Illumina sequencing, enabling high-throughput analysis.

Analysis of the CP29A CLIP dataset revealed 69 peaks in 15 chloroplast mRNAs and two tRNAs (Fig. 1A). CP33B CLIP identified 52 peaks among five mRNAs and one tRNA (*SI Appendix, Fig. S2A*). Importantly, no sequence-level overlap was observed between significantly enriched peaks in the CP29A and CP33B datasets, indicating distinct specificities. CP33B's main target was the *psbA* mRNA, whereas *rbcl* mRNA was a strong target of CP29A (Fig. 1A and B and *SI Appendix, Table S1*), consistent with previous analyses (3, 14, 15).

CP29A peaks were called in all transcriptional units encoding proteins of the photosystem II complex (*psbB-psbT-psbH-petB-petD; psbD-psbC-psbZ; psbE-psbF-psbL-psbJ; psbK-psbI; psbM*), except in the monocistronic *psbN* and *psbA* mRNAs (Fig. 1A). CP29A also targeted *atpF* mRNA along with monocistronic mRNAs *psal*, *petN*, and *rbcl*. Most significant CP29A peaks were within coding sequences, along with peaks in tRNA genes *trnH* and *trnT* and several peaks in 3' and 5' untranslated regions (UTRs). UTRs are known to be of prime importance for the regulation of transcript stability and translation in chloroplasts (16) and are therefore of special interest. Target UTRs of CP29A include the 3'-UTRs of *atpF* (partly overlapping with the CDS), *petN*, *psbM*, and the 5'-UTR of *rbcl* and *petB* (Fig. 1B and *SI Appendix, Fig. S3 A–F*).

For CP33B, significant peaks were also predominantly located in the CDS of target genes (Fig. 1B and *SI Appendix, Fig. S3 D–F*, except for *atpH*, where peaks extended partially into the 3' UTR (*SI Appendix, Fig. S3C*). Besides the top peak in *psbA*, peaks were identified in the second exon of *petB*, in *psbB* and *psbD* mRNA, and in *atpH* (*SI Appendix, Figs. S2 A and C and S3 C–F*).

It is essential to acknowledge potential bias in CLIP analysis for CP29A and CP33B, favoring well-expressed genes. All target genes rank in the top two tertiles based on read counts in wt Col-0 RNA-sequencing (RNA-seq) datasets (17). Consequently, there is a risk of false negatives due to low expression levels, possibly affecting intronic regions. The identified transcripts in CP29A and CP33B datasets through CLIP align with previously identified target mRNAs (3, 14, 15), highlighting the utility of CLIP-based assays in chloroplasts.

In Vitro Binding Data Reveal the Sequence Specificity of CP29A and CP33B.

We employed the in vitro method RNA Bind-n-Seq [RBNS; (18)] to supplement in vivo CLIP data. RBNS uses recombinant RBPs to enrich and identify their sequence motifs from a synthesized pool of random RNAs, utilizing high-throughput sequencing. To this end, CP29A and CP33B were genetically modified with an N-terminal glutathione-S-transferase (GST) tag and a streptavidin-binding protein (SBP) tag, expressed in *Escherichia coli*, and purified via the GST tag. After removal of the GST-tag, purified RBPs were incubated at different concentrations (0, 10, 100, and 1,000 nM) with a pool of random 40-mer RNA oligonucleotides. After pulldown using the SBP tag, RBP-associated RNAs were isolated. We prepared and sequenced libraries from both the random RNA input pool and the immunoprecipitated RNAs using Illumina sequencing, resulting in approximately 20 million reads per library. Utilizing the RBNS pipeline (19), we counted all possible k-mers of a specified length in both the IP samples and the input RNA pool and calculated the enrichment of each k-mer as its frequency in the IP samples relative to its frequency in the input pool, denoted as the R-value.

Given that RRM domains typically bind sequences ranging from 2 to 4 nucleotides and that cpRNPs contain two RRM domains, we focused our RBNS library analysis on 6-mers. The highest R-values for both CP29A and CP33B were found in libraries derived from IPs conducted with a protein concentration of 100 nM. Control samples without protein lacked significant 6-mer enrichment. For CP29A, the highest enriched 6-mers were UUUUUU (R = 2.26), UUUUUA (R = 1.98), and UAUUUU (R = 1.97). CP33B's highest enriched 6-mers were GUUACU (R = 3.47), GGUUAC (R = 3.39), and GCUACU (R = 2.67). These k-mers were consistently identified as top k-mers across tested protein concentrations. The set of significantly enriched 6-mers of each RBP were used to construct consensus sequence motifs and corresponding position weight matrices (Fig. 1C and *SI Appendix, Fig. S2B*).

The binding preference of CP29A was most accurately characterized by a degenerate U-rich motif, with A, U, or G being almost equally probable at the third position. The position weight matrix (PWM)-based consensus motif for CP33B corresponded closely to the consensus sequence GHUAUY. We next explored the role of individual RRM domains in binding to U-rich RNA motifs. We monitored the NMR chemical shifts of amides upon titration of a “UUUUUUU” RNA oligonucleotide to the individual ¹⁵N-labeled CP29A RRM domains. RRM1 exhibited more pronounced chemical shift perturbations (CSPs) upon binding to UUUUUUU RNA compared to RRM2 (Fig. 1E and F). When mapping the CSP onto structural models of the two RRMs, the two RNP sequence motifs are strongly affected, suggesting that the CP29A RRMs exhibit a canonical interaction with the RNA (Fig. 1F). However, the RNA binding affinities estimated from the NMR titrations are different for both RRMs, where RRM2 shows weaker interactions than the RRM1. Overall, RBNS experiments and NMR-based assays of CP29A binding indicate that U-rich sequences are the primary targets of CP29A. To assess the binding of the CLIP-derived motifs for CP29A, we performed

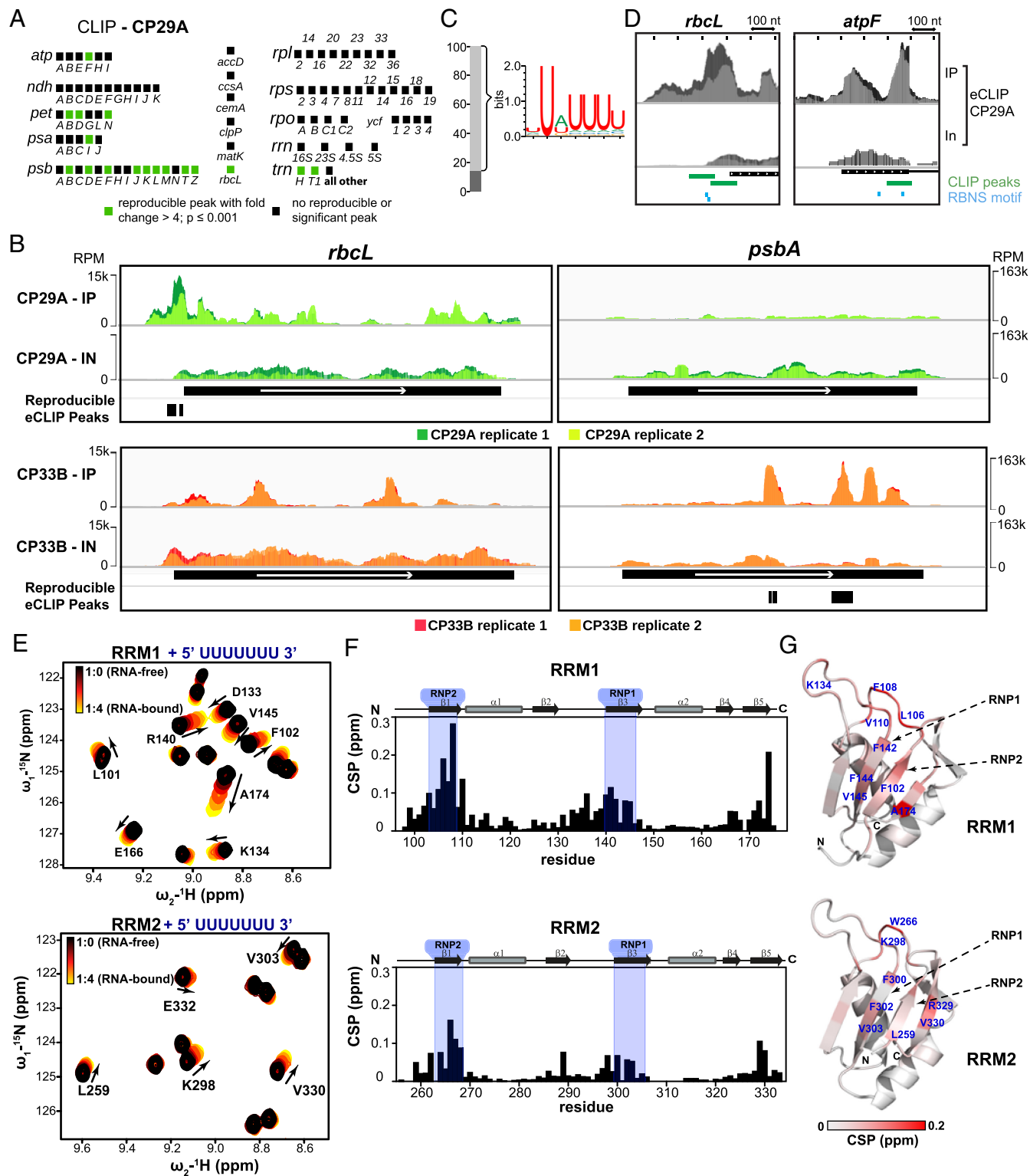


Fig. 1. RNA binding analysis of CP29A. (A) Summary of reproducible eCLIP peaks for CP29A. eCLIP libraries (IP) and corresponding size-matched input (IN) libraries were prepared from UV-cross-linked chloroplasts. The library preparation workflow was adapted to chloroplasts based on the eCLIP protocol (12). Data analysis was performed using the eCLIP pipeline (v0.3.99) and the chloroplast genome (TAIR10; customized AtRTD2 annotation with designated 100 nt of 5'- and 3'-UTR). Identified peaks were considered significant and reproducible if fold enrichment was >4 and $P < 0.001$ in eCLIP versus size-matched input, in both replicates. (B) Detailed CLIP data for CP29A and CP33B at the *rbcL* and *psbA* locus. Read coverage (in reads per million = RPM) plots are shown for both biological replicates. Reproducible peaks are annotated as black rectangles. (C) Sequence preferences of CP29A were analyzed using the RNA Bind-N-Seq method. Significantly enriched 6-mers were used to construct a sequence logo, which represents most of the observed binding of CP29A. (D) Examples of overlapping RBNS motifs and eCLIP peaks are shown for CP29A in *rbcL* and *atpF*. (E) Overlays of ¹H-¹⁵N NMR correlation spectra of the RRM1 (Upper graph) and RRM2 (Lower graph) domains of CP29A with increasing concentration of "UUUUUUU" RNA oligonucleotide. Chemical shift changes upon RNA binding are highlighted with arrows. (F) Chemical shift perturbations (CSP) for RRM1 (Upper graph) and RRM2 (Lower graph) in the presence of fourfold excess of RNA are shown. The secondary structure of the RRMs is indicated and the RNP motifs are highlighted in blue. (G) The change in chemical shifts are mapped onto the structural model of individual RRMs with gray to red color gradient. The RNA binding surface is highlighted in red and the key residues involved in RNA interactions are indicated.

NMR titrations with short single-stranded DNA oligonucleotides, as we expect that binding specificity of these oligos resembles corresponding RNA ligands (*SI Appendix, Fig. S4 A and B*). Analysis of the NMR titrations indicated strongest binding of “TGTTTT” and “TTTTTT” oligos to RRM1. On the other hand, RRM2 of CP29A shows the strongest response with TGTTTT and “GTTACT” oligos (*SI Appendix, Fig. S4 C and D*). These findings indicate that the RRM1 and RRM2 primarily recognize “T-rich” sequences, mainly “TTT” and “GTT” motifs (*SI Appendix, Fig. S4C*), well in line with our CLIP and RBNS binding analysis.

To assess the occurrence of the RBNS-derived consensus motifs within CLIP peaks versus control peaks, we utilized the Analysis of Motif Enrichment (AME) tool from the MEME suite (20). CLIP-derived peaks within 10 base pairs were merged and extended to match the largest peak size (53 nucleotides for CP29A, 82 for CP33B). The control peak set was created by shuffling all chloroplast sequences used in the CLIP analysis, ten times, resulting in ten random versions for each gene. From these, 1,000 peaks, matching the largest CLIP peak size, were used as a control set for the analysis of each RBP motif. Additionally, chloroplast gene sequences were employed to establish a 0-order background model for the AME tool.

The CP29A PWM-based RBNS motif was statistically significant (adjusted P -value < 0.05) enriched in 13 of 23 CLIP-derived merged peaks, for example, in *atpF* (Fig. 1D). Notably, this motif appeared twice in the *rbcl* 5'-UTR CLIP peak, which exhibited the lowest P -value in the peak enrichment analysis (Fig. 1D). In contrast, CP33B AME analysis did not reveal significant enrichment of the RBNS motif in merged CLIP peaks. However, this motif was found in 5 of the 8 merged peaks, including the *petB* and the *psbA* CLIP peak, which had the lowest P -value in the CP33B CLIP analysis (*SI Appendix, Fig. S2C*).

The correlation between the sequence preferences of CP29A and CP33B identified by RBNS and their respective *in vivo* binding sites revealed through CLIP provides a foundation for establishing a high-confidence set of binding sites for both proteins.

CP29A Binds Adjacent to the Predicted Binding Sites of the PPR Protein MRL1 in the *rbcl* 5'-UTR. CP29A binds to several chloroplast RNAs, and it may play a role for all of them. However, in this work, we will focus on the binding site with the strongest statistical support, which was identified in the 5' UTR of the *rbcl* gene (Fig. 1B and *SI Appendix, Table S1*). Notably, *rbcl* was also the most strongly enriched RNA in previous RIP-slot-blot analyses of CP29A (3). A crucial factor known to influence the expression of *rbcl* is the PPR protein MRL1 (2). PPR proteins are known to produce short RNA fragments that are protected from nuclease degradation due to their tight binding (21–23). We previously discovered a short RNA fragment, designated as C28, which precisely matches the end of the mature, 5'-processed *rbcl* mRNA (21, 22). The formation of the processed 5' end of the *rbcl* RNA is dependent on the PPR protein MRL1 (2).

To assess MRL1's role in *rbcl* 5' sRNA/C28 sRNA accumulation, we performed small RNA (sRNA) sequencing on the *Arabidopsis mrl1* mutant, comparing it with wild-type (wt) plants. Our analysis identified C28 as the sole sRNA exhibiting differential accumulation across the plastid transcriptome (Fig. 2 A and B). Validation via RNA gel blot hybridization supported this finding (Fig. 2C). Control mutants lacking the PPR protein HCF152 or the H-TRP protein HCF107 accumulated the *rbcl* 5' footprint with a slight signal reduction (Fig. 2C). This decrease was attributed to pleiotropic effects stemming from their photosynthetic

defects. These controls substantiate the specificity of C28 loss observed in *mrl1* mutants.

The binding site of MRL1 within the *rbcl* mRNA was hypothesized to be near its 5'-end (2). Using the PPR code (24), we predicted MRL1's binding sequence based on the specific amino acids in each repeat of its PPR tract to align partially with the 5'-*rbcl* sRNA (Fig. 2D), corroborating the region proposed earlier (2). However, the sRNA extends considerably beyond this binding site. Interestingly, when analyzing the CP29A CLIP-data, we noticed that one peak is close to the MRL1-dependent C28 sRNA. Reads from eCLIP terminate at the protein–RNA cross-link site, providing base-specific resolution. Mapping read ends showed a peak downstream of the predicted MRL1 site, still within the C28 sRNA (Fig. 2D). This alignment is notable as the U-rich target sequence in the *rbcl* peak aligns with the consensus sequence from our RBNS analysis (Figs. 1C and 2D). This suggests a potential functional overlap in the binding regions of MRL1 and CP29A within the *rbcl* mRNA, with CP29A binding downstream of the MRL1 site.

Arabidopsis CP29A Mutants Do Not Show a Change in *rbcl* mRNA Levels, nor Is Translation of the *rbcl* mRNA Reduced.

Considering MRL1's role in stabilizing and translating *rbcl* (2), we studied *rbcl* expression in *cp29a* null mutants under standard and cold acclimation conditions. We treated the plants for 3 d with 12 °C, conditions that do not yet lead to a photosynthetic or macroscopic phenotype, thus avoiding secondary effects due to failed chloroplast biogenesis (17). We found no significant alterations in *rbcl* mRNA accumulation or RbcL protein levels between wt and *cp29a* mutants under either condition (*SI Appendix, Fig. S5 A–D*). As RuBisCo has a long half-life of 7 d (25, 26), smaller changes on the level of translation activity may not become visible after 3 d on the backdrop of the large pool of stable RuBisCo protein. We therefore next tested the synthesis of chloroplast proteins by labeling with 35S methionine. After 3 d of cold exposure, no significant alterations were detected in protein synthesis of either RbcL or D1 as a control protein in the chloroplasts of the *Arabidopsis cp29a* null mutants (*SI Appendix, Fig. S5 E–H*). These findings suggest that CP29A absence does not notably affect *rbcl* mRNA accumulation or translation in short-term cold-treated *Arabidopsis* tissue.

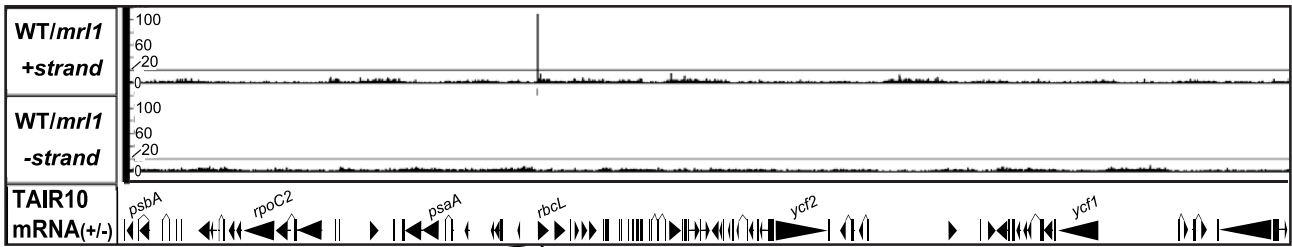
CRISPR-Cas9-Induced Null Mutants of Tobacco CP29A Show Photosynthetic Deficiency in the Cold.

Arabidopsis thaliana, a cold-adapted species, thrives in temperate zones and can grow even at 4 °C. We asked whether the disruption of a CP29A relative in tobacco (*NtCP29A*), a tropical plant, which does not often need to acclimate to cold, might yield similar outcomes. This choice was informed by evidence showing that *NtCP29A* localizes to the chloroplast, can bind *rbcl* and other RNAs *in vitro* and *in vivo* (5, 27), and stabilize RNAs *in vitro* (28), mirroring some of the functions of CP29A in *A. thaliana*.

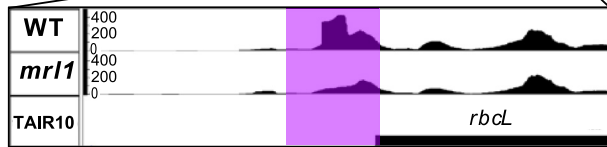
Tobacco, an allotetraploid derived from *N. sylvestris* and *N. tomentosiformis*, harbors two sets of alleles denoted here as *NtsCP29A* and *NttCP29A*. Utilizing CRISPR/Cas9 mutagenesis, we targeted all four alleles to generate null mutants (*SI Appendix, Fig. S6A*). In the T1 generation, we obtained plants lacking either *NtsCP29A* or *NttCP29A*, but not plants with large deletions in both alleles. After self-fertilization and crossing, we generated a homozygous *Ntscp29a/Nttcp29a* line, confirmed by PCR (*SI Appendix, Fig. S6B*) and sequencing (*SI Appendix, Fig. S6C*). We designate these plant lines as *Ntcp29a* mutants.

Under standard conditions, *Ntcp29a* plants resembled the wild type, showing no abnormalities (*SI Appendix, Fig. S6D*). After 7

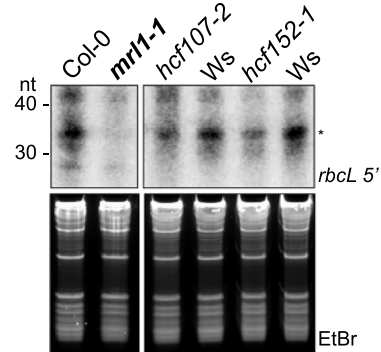
A



B



C



D

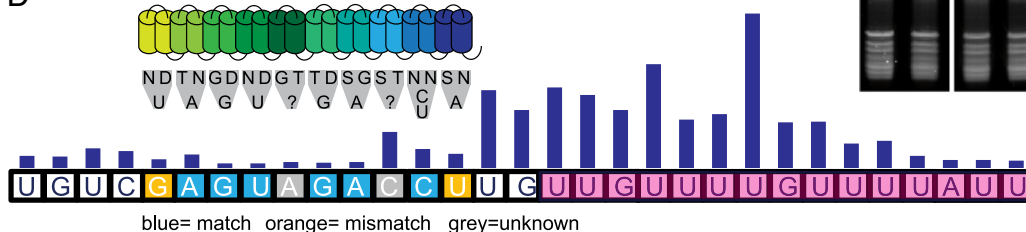


Fig. 2. Identification of differential sRNA accumulation in *mrl1* mutants. (A) Ratios of wt and mutant sRNA sequencing counts. Ratios for the positive and negative strands are shown for the 5' end of sRNAs. Only for the sRNA C28 in the *rbcl* 5'UTR, a high ratio of reads in wt versus *mrl1* was identified. (B) An sRNA coverage graph of the corresponding genomic region is shown here. The area of differential RNA accumulation is shaded in violet. (C) sRNA gel blot analysis of C28 in *mrl1* mutants and the corresponding wt were grown on soil for 3 wk. The *high chlorophyll fluorescence* (*hcf*) mutants *hcf107-2* and *hcf152-1* were analyzed as controls with known sRNA accumulation defects. Since these mutants are in the Wassilewskija (Ws) background, Ws plants were used as control. (D) Mapping of the predicted MRL binding site, CP29A eCLIP data and CP29A RBNS data onto the *rbcl* sRNA C28 sequence. The sequence of C28 is shown with framed capital letters. MRL1 has 10 PPRs, which are schematically shown as an array of two joined helices. The key amino acids are shown below together with their predicted base target. CP29A eCLIP-coverage data of read termini are shown as a bar graph above the bases in the sRNA sequence. The bases matching the RBNS consensus shown in Fig. 1C are highlighted in magenta.

d of low temperatures, they still displayed no macroscopic defects (*SI Appendix*, Fig. S6D). Given that *Atcp29a* mutants experience photosynthetic impairments under prolonged cold exposure (17), we evaluated the maximum quantum yield efficiency of photosystem II in *Ntcp29a* mutants. The Fv/Fm values were slightly decreased under normal conditions, worsening significantly in the cold compared to the wild type (Fig. 3 A and B). This decline resembles observations in *Arabidopsis* mutants. Notably, while *Atcp29a* mutants showed reduced Fv/Fm only in young leaf tissue (Fig. 3C), *Ntcp29a* mutants exhibited decreased efficiency across entire leaves under both conditions (Fig. 3A).

We confirmed that the absence of *NtCP29A* caused the photosynthetic defect by a complementation test on the null mutant. Introduction of full-length genomic versions of both *N. sylvestris* and *N. tomentosiformis* alleles via *Agrobacterium*-mediated transformation resulted in restored photosynthetic activity (Fig. 3 A and B). Recovery levels varied across complementation lines, likely due to varying transgene expression levels. Overall, these analyses confirm that the tobacco *NtCP29A* is essential for maintaining full photosynthetic performance during cold acclimation.

Tobacco CP29A Mutants Have Reduced Levels of *rbcl* mRNA and RbcL Protein in the Cold. To identify the molecular cause of the diminished photosynthetic performance in *Ntcp29a* mutants, we examined chloroplast RNA processing and accumulation under normal growth conditions (21 d at 24 °C) and after exposure to cold (21 d at 24 °C + 7 d at 12 °C). At 12 °C, tobacco plants exhibit significantly reduced growth, becoming only marginally larger

than control plants after 7 d. Thus, the plants are comparable, having reached a similar developmental stage, unlike plants grown at 24 °C for 24 + 7 d, which would be developmentally far more advanced. RNA extraction was done from one-half of the fourth primary leaf, followed by Illumina-based RNA-seq after rRNA depletion. Protein analysis was done on the other half of the leaf (details below).

Considering that *Atcp29a* mutants exhibited splicing defects after short-term cold exposure before visible bleaching (17), we investigated RNA splicing in the tobacco mutants. Using the Chloro-Seq pipeline (29), we assessed the splicing efficiency of the 21 introns in the tobacco chloroplast genome. Our results showed no significant differences in splicing efficiency between the two genotypes under either normal or cold conditions (*SI Appendix*, Fig. S7 A and B). In addition, we quantified chloroplast RNA editing in wt and mutants under both conditions, again showing no significant changes (*SI Appendix*, Fig. S7 C and D).

Next, we investigated RNA accumulation differences between the two genotypes under normal and cold temperatures. Sequencing results were analyzed using the DeSeq2 pipeline (30). Principal component analysis (PCA) showed good clustering of replicates (Fig. 4A), with the first principal component differentiating growth conditions, while the second, much smaller component reflected the variance between mutant and wt samples (Fig. 4A). This aligns with the expected impact of cold on RNA pools, resulting in marked differences in transcript accumulation.

We compared chloroplast gene expression in *Ntcp29a* mutants to the wt, focusing on normalized RNA coverage fold changes.

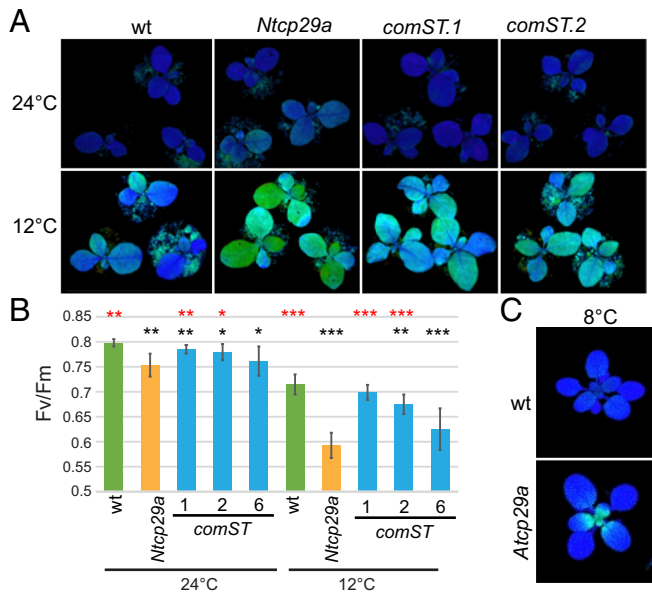


Fig. 3. Chlorophyll a fluorescence analysis of *Ntcp29a* mutants. (A) Visualization of the maximum quantum yield of photosystem II (Fv/Fm) with an imaging PAM under normal growth conditions and after cold treatment. Wt, *Ntcp29a* mutants, and three independent complementation lines (*comST*) were grown for 21 d at 24 °C and then transferred to 12 °C for 7 d. (B) Fv/Fm values based on the measurements of eight individual plants for each plant line. Bars indicate the SD and the asterisks represent the statistical significance (**P*-value < 0.05; ***P*-value < 0.01; ****P*-value < 0.001), as evaluated by Student's *t* test. red asterisks = comparison to *Ntcp29a* mutants; black asterisks = comparison to wt. (C) Phenotype of *Arabidopsis Atcp29a* mutants in comparison to wt after 14 d at 21 °C and 10 d at 8 °C.

Out of 94 genes meeting detection criteria, *rbcl* showed the strongest decrease, reaching 49% of wt levels, exclusively under cold conditions (Fig. 4 B and C). Expression changes occurred also in other genes, including eCLIP targets of CP29A, but none reached our fold change threshold. We also observed a comparable reduction of *rbcl* mRNA in RNA gel blot hybridization experiments (Fig. 4D). Overall, *Ntcp29a* mutants exhibited a significant and specific reduction in *rbcl* mRNA at low temperatures.

We next investigated whether the decrease in *rbcl* mRNA affected RbcL protein accumulation by immunoblot analyses. Apart from RbcL, we examined other subunits from the Photosystem I and II, the ATPase, and the cytochrome b6f complex. RbcL showed the strongest reduction in *Ntcp29a* mutants in the cold, to less than 50% of wt levels. Other proteins showed, albeit to a lesser extent, a downregulation as well (Fig. 4 E and F). This cold-specific reduction in RbcL levels can also be observed in Ponceau S-stains (Fig. 4E).

NtCP29A Affects *rbcl* RNA Processing But Not Translation in the Cold. To identify the molecular cause of the reduced *rbcl* levels in *Ntcp29a* mutants, we first investigated whether the tobacco NtCP29A protein associates with *rbcl* mRNA. For this purpose, we generated tobacco plants expressing a version of NtCP29A with green fluorescent protein (GFP) inserted between the targeting peptide and the rest of the coding region, in a *Ntcp29a* null mutant background. This tagging strategy has been successfully applied to *Arabidopsis* recently (17). We demonstrated through immunoblot analysis that the protein accumulates in the transgenic lines (SI Appendix, Fig. S8A). The NtGFP-CP29A expressing plants showed a partial recovery of their photosynthetic capacity (SI Appendix, Fig. S8B), indicating that the fusion protein can at least in part fulfill its molecular

functions. We next conducted RNA-coimmunoprecipitation experiments with NtGFP-CP29A. The NtGFP-CP29A protein was successfully recovered in the pellet fraction from three replicate immunoprecipitations (IPs) using chloroplast stroma preparations (SI Appendix, Fig. S9A). RNA from the pellet and supernatant fractions was analyzed by dot-blot hybridization (SI Appendix, Fig. S9B). This analysis revealed that *rbcl* mRNA is enriched in the IP samples compared to mock controls and that *rbcl* is more strongly enriched in CP29A IPs than the *psbA* mRNA, which our eCLIP data suggest is not a direct target of *Arabidopsis* CP29A (Fig. 5A). Additionally, we observed a trend indicating stronger binding to the UTR than to the coding region of *rbcl* (Fig. 5A). These results establish that the association of CP29A with *rbcl* mRNA is conserved between tobacco and *Arabidopsis* and suggest that the observed effects on *rbcl* RNA and RbcL protein levels in the mutant are direct consequence of the loss of CP29A.

The *rbcl* UTR is a known site of RNA processing activity with a primary transcript end and a processed form (31). MRL1 acts as an RNA stabilizer, protecting the *rbcl* mRNA against 5'-to-3' exonucleolytic decay by RNase J, which generates the processed end of the *rbcl* mRNA (2, 32). Furthermore, the *rbcl* UTR experiences heavy RNA processing in mutants lacking certain exonucleases (33). The loss of *rbcl* mRNA in *cp29a* mutants under cold conditions could be due to a failure to protect the RNA from degradation, possibly because a lack of support from CP29A for MRL1 binding to its target. To investigate this, we analyzed the 5'-ends of *rbcl* in cold-treated wt and mutant plants using RACE (Rapid Amplification of cDNA Ends). This led to the detection of the expected two main ends when amplification products were analyzed by gel electrophoresis (SI Appendix, Fig. S10). We then performed amplicon sequencing of the RACE products from cold-treated samples to identify possible changes due to aberrant transcript degradation in the mutant. Mapping of the 5'-ends of the RACE amplicon sequencing reads predominantly showed the canonical processed end in all samples (PE 1; Fig. 5 B and C). Additionally, we detected reads terminating 18 nucleotides upstream of PE 1, which we interpreted as a processing intermediate on the way from the primary transcript to PE 1 (we termed this end PE 2). Surprisingly, the ratio of PE 2 to PE 1 shifted significantly toward PE 1 in the mutant under cold conditions consistently across all three biological replicates (Fig. 5 B and D). This suggests that NtCP29A has a cold-dependent negative effect on the processing of *rbcl* mRNA upstream of the canonical processed 5'-end.

Given that UTR structure and processing are suggested to impact chloroplast translation, and since CP29A also has a binding site covering part of the *rbcl* Shine-Dalgarno sequence (Fig. 5C and SI Appendix, Table S1), we next analyzed translational activity by feeding leaves with radiolabeled methionine and measuring its incorporation into RbcL protein. While there is no significant change, there is a trend toward increased translational activity in the cold-treated *Ntcp29a* mutant (Fig. 5 E and F). In surprising contrast to the increase in translational activity, immunoblot analysis of the same blot confirms that the steady-state amount of RbcL protein is reduced in the mutant, consistent with the findings presented in Fig. 4 E and F. Finally, to control for RNA abundance, we extracted RNA from plants grown in parallel to those used for the in vitro translation assays and performed RNA gel blot hybridization. The results replicate the reduction in *rbcl* mRNA in the mutant under cold conditions (Fig. 5 G and H). In summary, NtCP29 does not act as an activator of translation but may have a mild repressive effect on translation, while it positively acts on RbcL protein and mRNA accumulation.

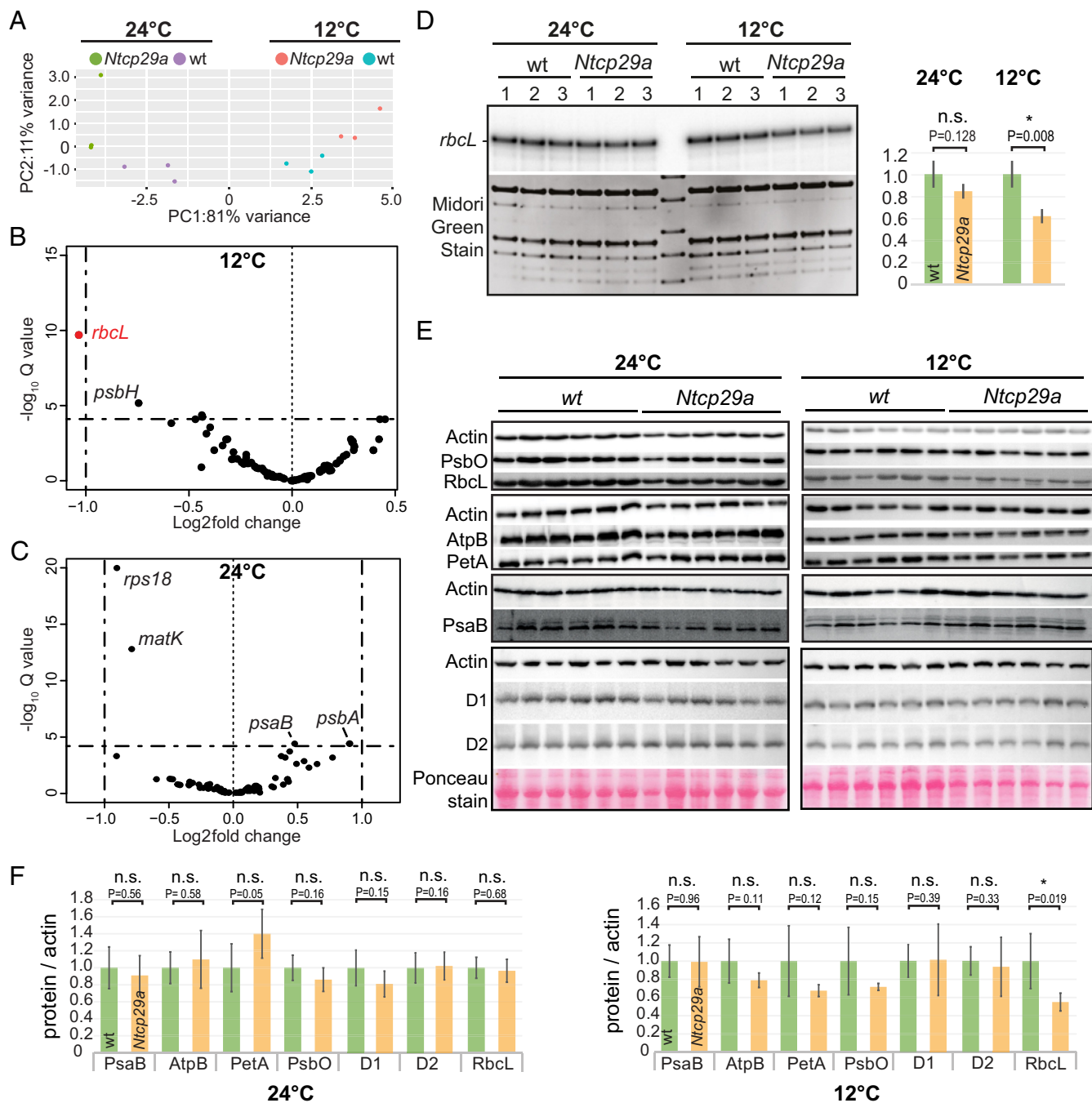


Fig. 4. Analysis of *rbcl* expression in *Ntcp29a* mutants. (A) PCA of *Ntcp29a* mutant and wt leaf RNA-Seq samples ($n = 3$). Plants were grown for 21 d at 24 °C and then directly analyzed or transferred for 7 d to 12 °C and then analyzed. (B) Volcano plot of RNA-Seq results for chloroplast RNAs from cold-treated mutant versus wt plants after cold treatment. Only the *rbcl* mRNA shows a more than twofold downregulation in the cold, which is statistically significant ($P < 0.001$; significance test: Wald test adjusted with Benjamini-Hochberg). Dashed lines show selected thresholds for fold change and Q value. (C) As in B, but for plants grown at standard growth temperature, 24 °C. No expression changes above the twofold threshold were detected. (D) RNA gel blot hybridization analysis was performed on total leaf RNA (normalized per gram of fresh weight) from specified tobacco lines using a radiolabeled *rbcl*-specific probe. A quantification of the autoradiograph signals is displayed on the Right. (E) Immunoblot analysis of leaf extracts of tobacco seedlings. Samples from plants analyzed for RNA accumulation in A-C were subject to immunological analyses, loading based on equal amounts of fresh weight. A total of six wt and six *Ntcp29a* mutant plants were analyzed. Multiple probedings of the same blot are boxed. A Ponceau S-stain highlighting the RbcL band is shown for only one immunoblot per growth temperature. (F) Quantification of immunoblot analysis from D. * $P < 0.05$; Student's *t* test.

Discussion

eCLIP Reveals a Posttranscriptional Operon Rich in PSII mRNAs for AtCP29A

In this study, we employed the eCLIP-Seq method to investigate RNA interactions of a chloroplast RBP. We demonstrate that despite high pigment concentrations in chloroplasts UV-cross-linking is efficient enough to allow precipitation of RBP:RNA complexes. Our analysis revealed highly specific, distinct peaks,

distinguishing between closely related cpRNPs, thereby enabling specific ligand identification for *AtCP29A*. This approach offers significant advantages over previous methods like RIP, which might capture larger RNA-protein complexes, obscuring specific interactions (3, 5). The eCLIP-based analysis corroborated previous findings, identifying CP29A as a chloroplast RBP with a multitude of target transcripts. This includes the reconfirmation of previously identified targets like *rbcl*, *psbD*, and *psbB*. Other previously

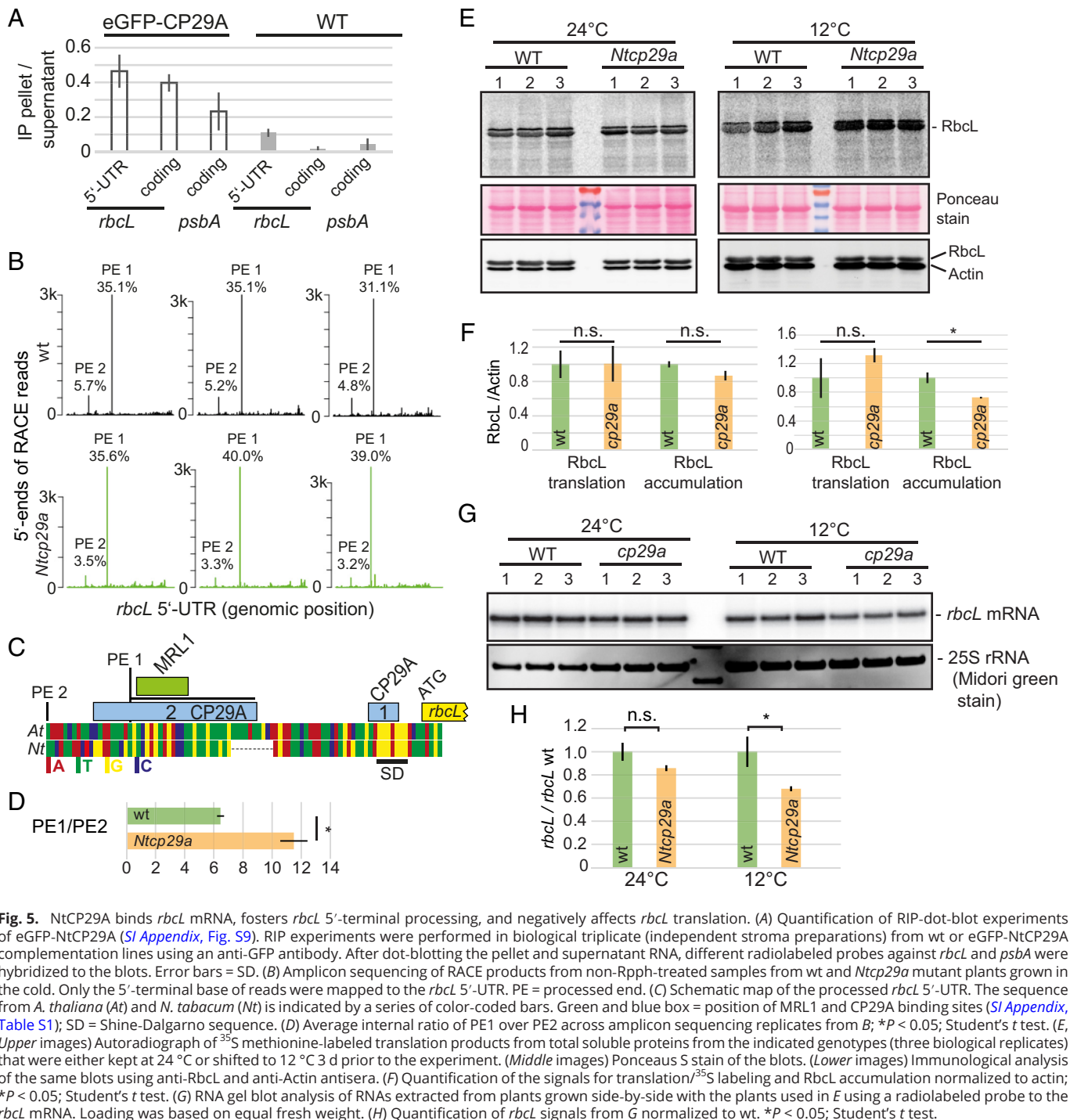


Fig. 5. NtCP29A binds *rbcL* mRNA, fosters *rbcL* 5'-terminal processing, and negatively affects *rbcL* translation. (A) Quantification of RIP-dot-blot experiments of eGFP-NtCP29A (SI Appendix, Fig. S9). RIP experiments were performed in biological triplicate (independent stroma preparations) from wt or eGFP-NtCP29A complementation lines using an anti-GFP antibody. After dot-blotting the pellet and supernatant RNA, different radiolabeled probes against *rbcL* and *psbA* were hybridized to the blots. Error bars = SD. (B) Amplicon sequencing of RACE products from non-Rpph-treated samples from wt and *Ntcp29a* mutant plants grown in the cold. Only the 5'-terminal base of reads were mapped to the *rbcL* 5'-UTR. PE = processed end. (C) Schematic map of the processed *rbcL* 5'-UTR. The sequence from *A. thaliana* (*At*) and *N. tabacum* (*Nt*) is indicated by a series of color-coded bars. Green and blue box = position of MRL1 and CP29A binding sites (SI Appendix, Table S1); SD = Shine-Dalgarno sequence. (D) Average internal ratio of PE1 over PE2 across amplicon sequencing replicates from B; * $P < 0.05$; Student's *t* test. (E, Upper images) Autoradiograph of ^{35}S methionine-labeled translation products from total soluble proteins from the indicated genotypes (three biological replicates) that were either kept at 24°C or shifted to 12°C 3 d prior to the experiment. (Middle images) Ponceau S stain of the blots. (Lower images) Immunological analysis of the same blots using anti-RbcL and anti-Actin antisera. (F) Quantification of the signals for translation/ ^{35}S labeling and RbcL accumulation normalized to actin; * $P < 0.05$; Student's *t* test. (G) RNA gel blot analysis of RNAs extracted from plants grown side-by-side with the plants used in E using a radiolabeled probe to the *rbcL* mRNA. Loading was based on equal fresh weight. (H) Quantification of *rbcL* signals from G normalized to wt. * $P < 0.05$; Student's *t* test.

identified targets were not identified in the current eCLIP analysis. This discrepancy could be attributed to the absence of fixed cutoff criteria in the earlier RIP-Chip experiments, suggesting that these genes might represent minor targets of CP29A. They possibly did not meet the more stringent threshold criteria applied in the present eCLIP experiment.

Many of these binding sites are in mRNAs coding for photosystem II subunits as well as for other photosynthetic electron transport components. For example, within the *psbB* operon, genes like *psbB*, *psbT*, *petB*, and *petD* were identified as targets. Similarly, in the *psbE* operon, *psbF*, *psbL*, and *psbJ* emerged as targets. This finding is particularly noteworthy because the input RNA in the eCLIP-based approach undergoes fragmentation during cell lysis,

and the resulting library is size-selected. This process allows for the differentiation of binding sites even within the same gene, as exemplified by the identification of distinct binding sites in the 5' UTR and exon 2 of *petB* (SI Appendix, Fig. S3B). Additionally to polycistronic photosystem II transcripts, the functionally related monocistronic transcripts of *psbM*, *psbK*, and *petN* were also identified as targets. The preferential association of AtCP29A with these functionally related transcripts suggests the potential existence of a posttranscriptional operon, a concept previously described in various species (34). Another cpRNP, AtCP31A has been demonstrated to associate preferentially with mRNAs encoding subunits of the NDH complex (35), which are not targets of AtCP29A. AtCP33B with its preference for the *psbA* mRNA that is neither

targeted by AtCP29A nor by AtCP31A has yet another nonoverlapping target range. Therefore, the data presented here suggest that cpRNPs might serve as operon-defining chloroplast RNA-binding proteins, indicating a sophisticated level of posttranscriptional regulation within the chloroplast.

While our study identified an intriguing target profile for AtCP29A, most of these mRNAs did not exhibit significant accumulation changes in previous RNA-Seq analyses conducted on *Atcp29a* mutants (17), nor in the RNA-Seq analysis of *Ntcp29a* mutants. However, many AtCP29A binding sites are within coding regions, suggesting a role in translation. Supporting this, Ribo-Seq analysis indicated reduced translation in *Atcp29a* mutants under cold conditions (17). Thus, while CP29A's direct impact on mRNA accumulation seems limited, its potential role in translation regulation or other subtle RNA processing aspects in *cp29a* mutants merits further investigation, especially concerning plant responses to cold stress. Recently, we demonstrated that CP29A can form granular structures at low temperatures through phase separation, which affects the splicing of specific chloroplast introns (17). Whether granule formation also plays a role for *rbcl* accumulation in tobacco remains to be determined. CP29A shows increased accumulation in the cold (3), suggesting that it may play a role in adjusting the output of chloroplast gene expression at multiple posttranscriptional levels.

Sequence Preferences of AtCP29A. The RBNS method unveiled the sequence preferences of cpRNPs, challenging previous notions of their nonspecificity (4). It unveiled consistent k-mer enrichments across all libraries associated with a specific cpRNP but not in the zero-protein control, validating RBNS specificity using recombinant cpRNPs. The identification of distinct target sequence motifs for CP29A and CP33B indicates that, although cpRNPs bind to many chloroplast RNAs, their binding is specific and not merely due to a general affinity for RNA. Notably, CP29A's enrichment of polyU motifs aligns with previous findings on tobacco homologs' U-binding ability (36). Since both RRM domains show a preference for U-rich sequences in our NMR-based RNA binding analysis, we speculate that CP29A can bind either longer U-stretches on single transcripts or can bridge two separate RNAs with U-rich motifs. Binding of nonconsecutive RNA motifs has been indeed observed in RBPs with multiple RRM domains (37, 38). The latter could be important for network formation during the described phase separation of CP29A, which depends on the prion-like linker domain between CP29A's two RRMs, but likely also requires the two RRMs themselves (17).

Extensive profiling of human RBPs revealed a preference for low-complexity target motifs (19). Given that chloroplast genomes typically have low GC content, the predominance of simple U or A binding motifs in chloroplast RBPs might represent an evolutionary adaptation. Such a motif could be functionally significant to coregulate multiple transcripts posttranscriptionally. In contrast to CP29A, CP33B binds to a more complex GHUAUY motif, potentially explaining its fewer target RNAs compared to CP29A and CP31A. This suggests that the complexity of binding motifs may influence the range of target RNAs an RBP can regulate.

Ntcp29A Supports *rbcl* Expression in the Cold in Tobacco. RNAs often interact with multiple RBPs that work together to regulate the expression or repression of their target transcripts. Many RBPs with RRM domains, such as twin RRM-proteins in the heterogeneous nuclear RNP (hnRNP) class, function in coordination with other RBPs (39). In this context, it was observed that a high-confidence eCLIP binding site on the *rbcl* mRNA in

chloroplasts is proximal to a region proposed for MRL1 protein targeting. Genetic analyses of *mrl1* mutants in *Chlamydomonas reinhardtii* and *Arabidopsis* (2), alongside predictions of MRL1-binding sites and identification of MRL1-dependent *rbcl* sRNA accumulation, imply MRL1 binding to the *rbcl* mRNA 5'-end near the AtCP29A binding site.

The proximity of the CP29A and MRL1 binding sites suggested a potential cooperative interaction between these proteins, prompting us to examine MRL1's known roles in 5'-end processing and translation of *rbcl* mRNA in *cp29a* mutants. Surprisingly, rather than impaired translation and 5'-end processing, we observed an increase in the accumulation of the MRL1-dependent processed PE 1 end and also in translational activity, both specifically under cold conditions. Thus, CP29A appears to act as an antagonist of MRL1 in the translation and 5'-end processing of *rbcl* mRNA in the cold. We hypothesize that loss of CP29A increases MRL1's ability to generate the PE 1 transcript end, possibly because of an easier access to the *rbcl* UTR. This antagonistic role of CP29A is reminiscent of structurally related nucleocytoplasmic hnRNPs, which are known to function as repressive factors in various gene expression steps, such as splicing [e.g., hnRNP A1/A2 and PTB, (40, 41)] and translation [e.g., hnRNP H/F; hnRNP Q1, (42, 43)]. The question remains: Why is there a significant reduction in steady-state RbcL levels in *Ntcp29a* mutants under cold conditions, even though the translation rate is not significantly decreased and may even be increased? Most parsimoniously, the RbcL protein produced in the mutant is unstable and subject to degradation. This could occur if RbcL is not incorporated into the RuBisCo holoenzyme, which consists of eight RbcL and eight nuclear-encoded RbcS subunits, and requires the assistance of several chaperones for assembly. Indeed, the depletion of RbcS has been shown to lead to the loss of RbcL through ClpP-dependent degradation (44, 45), and RbcL molecules that fail to achieve a productive conformation through chaperone interactions are targeted for degradation by proteases (46, 47). However, how CP29A's ability to bind to the *rbcl* mRNA could be linked to RbcL protein accumulation—in the absence of a role for *rbcl* translation—remains to be determined.

The anticipated outcome of a 50% reduction in RbcL, and consequently in RuBisCo, is a decrease in carbon fixation. Mutants with alterations in the catalytic center of RuBisCo (center is encoded by *rbcl*), as well as *rbcl* deletion mutants, exhibit pronounced photosynthetic deficiencies and associated growth defects (48, 49). Hypomorphic RuBisCo mutants caused by lowered RbcS levels show reduced Fv/Fm values similar to *Ntcp29a* plants, even at normal temperatures (50). However, we would like to emphasize that more direct effects on PSII expression could also contribute to the observed Fv/Fm reduction, especially given the binding sites found in PSII mRNAs. Plants grown in low temperatures typically exhibit higher concentrations and activities of RuBisCo and other enzymes involved in photosynthetic carbon metabolism than those grown at higher temperatures (51–54). This is supported in *Arabidopsis* by an increase of *rbcl* mRNA in the cold and a switch of nuclear-encoded RbcS gene isoforms (50, 55). The mechanisms underlying cold-dependent regulation of RuBisCo accumulation are poorly understood. However, it is clear that dedicated RuBisCo chaperones and feedback regulation play key roles in its general production. Specifically, the complex of the chaperone Raf1 with RbcL represses the translation of *rbcl* mRNA (44, 56), and both Raf1 and Raf2 are required for RuBisCo holoenzyme assembly (57, 58). Parallel overexpression of RbcL, RbcS, and Raf1 was shown to enhance cold tolerance in maize, demonstrating the critical role of RuBisCo expression in cold hardiness (59).

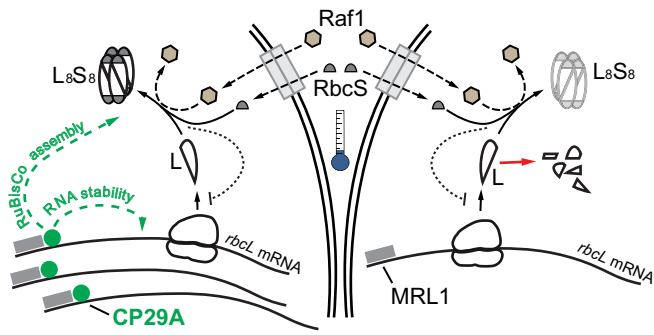


Fig. 6. Model of the function of CP29A in RbcL expression in the cold. (Left) CP29A binds to the 5'-UTR of the chloroplast *rbcL* mRNA downstream of the PPR protein MRL1. This stabilizes the mRNA. After translation of *rbcL*, the large subunit of RuBisCo (L) together with nuclear-encoded RbcS (S) is assembled into the L_8S_8 holoenzyme with the help of the chaperone Raf1 (and other chaperones not shown). The green arrows indicate positive effects of CP29A on RuBisCo assembly and *rbcL* mRNA stability, respectively. Blunt arrow: Assembly intermediates (L_8 -Raf1 complex) have been shown to act as a repressor of translation of *rbcL* in case RbcS is not available in *C. reinhardtii* (56). (Right) In *cp29a* null mutants, less *rbcL* mRNA accumulates in the cold, but translation rates remain as in WT. Since RbcL amounts are reduced in the *cp29a* mutant in the cold, we speculate that CP29A has a supportive role in RuBisCo assembly in the cold. If assembly is slowed down, excess RbcL is rapidly degraded.

How does CP29A fit into the regulation of RuBisCo production? While we demonstrate that CP29A supports the accumulation of *rbcL* mRNA, this accumulation is not limiting for RbcL translation (Fig. 5 E and F). Despite normal translation levels, the loss of CP29A still reduces steady-state levels of RbcL, suggesting a role for CP29A in stabilizing RbcL (Fig. 6). We can at present only speculate on potential mechanisms that could explain this stabilization. For example, CP29A might interfere directly with

proteolytic degradation or facilitate the incorporation of RbcL into the holoenzyme, where it is more stable than as an individual protein (46, 47). Given that multifactorial assembly processes are sensitive to low temperatures, we speculate that CP29A may contribute to the assembly of RbcL into the holoenzyme under cold conditions (Fig. 6). This can be tested by future studies on the assembly efficiency of RuBisCo in *cp29a* plants in the cold.

Materials and Methods

SI Appendix provides comprehensive details on the Materials and Methods utilized in this study. Within *SI Appendix, section I*, a thorough protocol for the chloroplast eCLIP method is outlined, along with specifics of the computational analysis performed. Details pertaining to RBNS are also included in *SI Appendix, section I*. Information regarding the NMR analysis can be found in *SI Appendix, section II*. *SI Appendix, section III* presents the CRISPR/Cas9 workflow that was followed. Furthermore, *SI Appendix, section IV* details the growth conditions and standard techniques employed in this study.

Data, Materials, and Software Availability. RNA Seq, eCLIP-SEQ, RBNS, eCLIP peaks for AtCP29A data have been deposited in SRA and GEO [PRJNA1043672 (60) and GSE248582 (61)].

ACKNOWLEDGMENTS. The vectors for CRISPR/Cas9 mutagenesis were kindly provided by Kerstin Kaufmann (HU Berlin). We are grateful to C. Stock (HU Berlin) for assistance in cultivation of tobacco tissue, genotyping, and immunoblotting. We thank Sam Asami and Gerd Gemmecker for support with NMR experiments. We acknowledge NMR facilities at the Bavarian NMR Center at the Technical University of Munich, Germany. We acknowledge SBGrid and the NMRbox server for providing access to NMR software. Portions of the paper were developed from the thesis of B.L. (10.18452/24203). This work was funded by DFG TR175 projects A02 to CSL and A07 to H.R.M.S. and C.S.-L. wish to acknowledge funding by DFG SPP1935 and DFG SPP2191.

- C. Crosatti, F. Rizza, F. W. Badeck, E. Mazzucotelli, L. Cattivelli, Harden the chloroplast to protect the plant. *Physiol. Plant.* **147**, 55–63 (2013).
- X. Johnson *et al.*, MRL1, a conserved pentatricopeptide repeat protein, is required for stabilization of *rbcL* mRNA in *Chlamydomonas* and *Arabidopsis*. *Plant Cell* **22**, 234–248 (2010).
- C. Kupsch *et al.*, *Arabidopsis* chloroplast RNA binding proteins CP31A and CP29A associate with large transcript pools and confer cold stress tolerance by influencing multiple chloroplast RNA processing steps. *Plant Cell* **24**, 4266–4280 (2012).
- Y. Q. Li, M. Sugiura, Nucleic acid-binding specificities of tobacco chloroplast ribonucleoproteins. *Nucleic Acids Res.* **19**, 2893–2896 (1991).
- T. Nakamura, M. Ohta, M. Sugiura, M. Sugita, Chloroplast ribonucleoproteins are associated with both mRNAs and intron-containing precursor tRNAs. *FEBS Lett.* **460**, 437–441 (1999).
- M. Teubner, J. Fuß, K. Kühn, K. Krause, C. Schmitz-Linneweber, The RNA recognition motif protein CP33A is a global ligand of chloroplast mRNAs and is essential for plastid biogenesis and plant development. *Plant J.* **89**, 472–485 (2017).
- D. D. Licatalosi *et al.*, HITS-CLIP yields genome-wide insights into brain alternative RNA processing. *Nature* **456**, 464–469 (2008).
- K. Meyer *et al.*, Adaptation of iCLIP to plants determines the binding landscape of the clock-regulated RNA-binding protein AtGRP7. *Genome Biol.* **18**, 204 (2017).
- J. König *et al.*, iCLIP-transcriptome-wide mapping of protein-RNA interactions with individual nucleotide resolution. *J. Vis. Exp.* **50**, e2638 (2011), 10.3791/2638.
- Y. Zhang *et al.*, Integrative genome-wide analysis reveals HLP1, a novel RNA-binding protein, regulates plant flowering by targeting alternative polyadenylation. *Cell Res.* **25**, 864–876 (2015).
- M. Reichel *et al.*, In planta determination of the mRNA-binding proteome of *Arabidopsis* etiolated seedlings. *Plant Cell* **28**, 2435–2452 (2016).
- E. L. Van Nostrand *et al.*, A large-scale binding and functional map of human RNA-binding proteins. *Nature* **583**, 711–719 (2020).
- E. L. Van Nostrand *et al.*, Robust transcriptome-wide discovery of RNA-binding protein binding sites with enhanced CLIP (eCLIP). *Nat. Methods* **13**, 508–514 (2016).
- K. P. Watkins *et al.*, Exploring the proteome associated with the mRNA encoding the D1 reaction center protein of Photosystem II in plant chloroplasts. *Plant J.* (2019), 10.1111/tpj.14629.
- M. Teubner *et al.*, The chloroplast ribonucleoprotein CP33B quantitatively binds the *psbA* mRNA. *Plants* **9**, 367 (2020).
- I. Small, J. Melonek, A.-V. Bohne, J. Nickelsen, C. Schmitz-Linneweber, Plant organellar RNA maturation. *Plant Cell* **35**, 1727–1751 (2023).
- J. Legen *et al.*, The prion-like domain of the chloroplast RNA binding protein CP29A is required for cold-induced phase separation next to nucleoids and supports RNA splicing and translation during cold acclimation. *Plant Cell* **36**, 2851–2872 (2024).
- N. Lambert *et al.*, RNA Bind-n-Seq: Quantitative assessment of the sequence and structural binding specificity of RNA binding proteins. *Mol. Cell* **54**, 887–900 (2014).
- D. Dominguez *et al.*, Sequence, structure, and context preferences of human RNA binding proteins. *Mol. Cell* **70**, 854–867.e9 (2018).
- R. C. McLeay, T. L. Bailey, Motif enrichment analysis: A unified framework and an evaluation on ChIP data. *BMC Bioinformatics* **11**, 165 (2010).
- H. Ruwe, C. Schmitz-Linneweber, Short non-coding RNA fragments accumulating in chloroplasts: Footprints of RNA binding proteins? *Nucleic Acids Res.* **40**, 3106–3116 (2012).
- H. Ruwe, G. Wang, S. Gusewski, C. Schmitz-Linneweber, Systematic analysis of plant mitochondrial and chloroplast small RNAs suggests organelle-specific mRNA stabilization mechanisms. *Nucleic Acids Res.* **44**, 7406–7417 (2016).
- J. Pfalz, O. A. Bayraktar, J. Prikyr, A. Barkan, Site-specific binding of a PPR protein defines and stabilizes 5' and 3' mRNA termini in chloroplasts. *EMBO J.* **28**, 2042–2052 (2009).
- A. Barkan *et al.*, A combinatorial amino acid code for RNA recognition by pentatricopeptide repeat proteins. *PLoS Genet.* **8**, e1002910 (2012).
- M. Piques *et al.*, Ribosome and transcript copy numbers, polysome occupancy and enzyme dynamics in *Arabidopsis*. *Mol. Syst. Biol.* **5**, 314 (2009).
- E. Simpson, Measurement of protein degradation in leaves of zea mays using [³H]acetic anhydride and tritiated water. *Plant Physiol.* **67**, 1214–1219 (1981).
- L. H. Ye *et al.*, Diversity of a ribonucleoprotein family in tobacco chloroplasts: Two new chloroplast ribonucleoproteins and a phylogenetic tree of ten chloroplast RNA-binding domains. *Nucleic Acids Res.* **19**, 6485–6490 (1991).
- T. Nakamura, M. Ohta, M. Sugiura, M. Sugita, Chloroplast ribonucleoproteins function as a stabilizing factor of ribosome-free mRNAs in the stroma. *J. Biol. Chem.* **276**, 147–152 (2001).
- B. Castandet, A. M. Hottot, S. R. Strickler, D. B. Stern, ChloroSeq, an optimized chloroplast RNA-seq bioinformatic pipeline, reveals remodeling of the organellar transcriptome under heat stress. *G3 (Bethesda)* **6**, 2817–2827 (2016).
- M. I. Love, W. Huber, S. Anders, Moderated estimation of fold change and dispersion for RNA-seq data with DESeq2. *Genome Biol.* **15**, 550 (2014).
- J. E. Mullet, E. M. Orozco Jr., N. H. Chua, Multiple transcripts for higher plant *rbcL* and *atpB* genes and localization of the transcription initiation site of the *rbcL* gene. *Plant Mol. Biol.* **4**, 39–54 (1985).
- S. Luro, A. Germain, R. E. Sharwood, D. B. Stern, RNase J participates in a pentatricopeptide repeat protein-mediated 5' end maturation of chloroplast mRNAs. *Nucleic Acids Res.* **41**, 9141–9151 (2013).
- B. Castandet, A. Germain, A. M. Hottot, D. B. Stern, Systematic sequencing of chloroplast transcript termini from *Arabidopsis thaliana* reveals >200 transcription initiation sites and the extensive imprints of RNA-binding proteins and secondary structures. *Nucleic Acids Res.* **47**, 11889–11905 (2019).
- J. D. Keene, RNA regulons: Coordination of post-transcriptional events. *Nat. Rev. Genet.* **8**, 533–543 (2007).
- B. Lenzen *et al.*, The chloroplast RNA binding protein CP31A has a preference for mRNAs encoding the subunits of the chloroplast NAD(P)H dehydrogenase complex and is required for their accumulation. *Int. J. Mol. Sci.* **21**, 5633–5646 (2020).
- L. Ye, M. Sugiura, Domains required for nucleic acid binding activities in chloroplast ribonucleoproteins. *Nucleic Acids Res.* **20**, 6275–6279 (1992).

37. F. E. Loughlin *et al.*, The solution structure of FUS bound to RNA reveals a bipartite mode of RNA recognition with both sequence and shape specificity. *Mol. Cell* **73**, 490–504.e6 (2019).
38. G. Dorn *et al.*, Structural modeling of protein-RNA complexes using crosslinking of segmentally isotope-labeled RNA and MS/MS. *Nat. Methods* **14**, 487–490 (2017).
39. S. P. Han, Y. H. Tang, R. Smith, Functional diversity of the hnRNPs: Past, present and perspectives. *Biochem. J* **430**, 379–392 (2010).
40. Y. Xue *et al.*, Genome-wide analysis of PTB-RNA interactions reveals a strategy used by the general splicing repressor to modulate exon inclusion or skipping. *Mol. Cell* **36**, 996–1006 (2009).
41. H. L. Okunola, A. R. Krainer, Cooperative-binding and splicing-repressive properties of hnRNP A1. *Mol. Cell. Biol.* **29**, 5620–5631 (2009).
42. K. R. Williams *et al.*, hnRNP-Q1 represses nascent axon growth in cortical neurons by inhibiting Gap-43 mRNA translation. *Mol. Biol. Cell* **27**, 518–534 (2016).
43. Y. Kalifa, T. Huang, L. N. Rosen, S. Chatterjee, E. R. Gavis, Glorund, a Drosophila hnRNP F/H homolog, is an ovarian repressor of nanos translation. *Dev. Cell* **10**, 291–301 (2006).
44. K. Wostrikoff, D. Stern, Rubisco large-subunit translation is autoregulated in response to its assembly state in tobacco chloroplasts. *Proc. Natl. Acad. Sci. U.S.A.* **104**, 6466–6471 (2007).
45. W. Majeran, K. Wostrikoff, F.-A. Wollman, O. Vallon, Role of ClpP in the biogenesis and degradation of RuBisCO and ATP synthase in *Chlamydomonas reinhardtii*. *Plants* **8**, 191–213 (2019).
46. G. W. Schmidt, M. L. Mishkind, Rapid degradation of unassembled ribulose 1,5-bisphosphate carboxylase small subunits in chloroplasts. *Proc. Natl. Acad. Sci. U.S.A.* **80**, 2632–2636 (1983).
47. R. J. Spreitzer, M. Goldschmidt-Clermont, M. Rahire, J. D. Rochaix, Nonsense mutations in the *Chlamydomonas* chloroplast gene that codes for the large subunit of ribulosebisphosphate carboxylase/oxygenase. *Proc. Natl. Acad. Sci. U.S.A.* **82**, 5460–5464 (1985).
48. S. M. Whitney, S. von Caemmerer, G. S. Hudson, T. J. Andrews, Directed mutation of the Rubisco large subunit of tobacco influences photorespiration and growth. *Plant Physiol.* **121**, 579–588 (1999).
49. Y. Allahverdiyeva, F. Mamedov, P. Mäenpää, I. Vass, E.-M. Aro, Modulation of photosynthetic electron transport in the absence of terminal electron acceptors: Characterization of the *rbcl* deletion mutant of tobacco. *Biochim. Biophys. Acta* **1709**, 69–83 (2005).
50. S. Donovan, Y. Mao, D. J. Orr, E. Carmo-Silva, A. J. McCormick, CRISPR-Cas9-Mediated mutagenesis of the Rubisco small subunit family in *Nicotiana tabacum*. *Front. Genome Ed.* **2**, 605614 (2020).
51. M. R. Badger, O. Björkman, P. A. Armond, An analysis of photosynthetic response and adaptation to temperature in higher plants: Temperature acclimation in the desert evergreen *Nerium oleander* L*. *Plant Cell Environ.* **5**, 85–99 (1982).
52. A. S. Holaday, W. Martindale, R. Alred, A. L. Brooks, R. C. Leegood, Changes in activities of enzymes of carbon metabolism in leaves during exposure of plants to low temperature. *Plant Physiol.* **98**, 1105–1114 (1992).
53. V. M. Hurry, O. Keerberg, T. Pärnik, P. Gardeström, G. Öquist, Cold-hardening results in increased activity of enzymes involved in carbon metabolism in leaves of winter rye (*Secale cereale* L.). *Planta* **195**, 554–562 (1995).
54. A. Strand *et al.*, Acclimation of Arabidopsis leaves developing at low temperatures. Increasing cytoplasmic volume accompanies increased activities of enzymes in the Calvin cycle and in the sucrose-biosynthesis pathway. *Plant Physiol.* **119**, 1387–1398 (1999).
55. A. P. Cavanagh, R. Slattery, D. S. Kubien, Temperature-induced changes in Arabidopsis Rubisco activity and isoform expression. *J. Exp. Bot.* **74**, 651–663 (2023).
56. W. Wietrzynski, E. Traverso, F.-A. Wollman, K. Wostrikoff, The state of oligomerization of Rubisco controls the rate of synthesis of the Rubisco large subunit in *Chlamydomonas reinhardtii*. *Plant Cell* **33**, 1706–1727 (2021).
57. K. Eshenour, A. Hotta, E. J. S. Michel, Z. G. Oh, D. B. Stern, Transgenic expression of Rubisco accumulation factor2 and Rubisco subunits increases photosynthesis and growth in maize. *J. Exp. Bot.* **75**, 4024–4037 (2024).
58. L. Feiz *et al.*, Ribulose-1,5-bis-phosphate carboxylase/oxygenase accumulation factor1 is required for holoenzyme assembly in maize. *Plant Cell* **24**, 3435–3446 (2012).
59. C. E. Salesse-Smith, R. E. Sharwood, F. A. Busch, D. B. Stern, Increased Rubisco content in maize mitigates chilling stress and speeds recovery. *Plant Biotechnol. J.* **18**, 1409–1420 (2020).
60. B. Lenzen, Role of chloroplast RNA binding protein CP29A for *rbcl* expression during cold acclimation. National Center for Biotechnology Information. <https://www.ncbi.nlm.nih.gov/bioproject/?term=PRJNA1043672>. Deposited 21 November 2023.
61. F. Rösch, NtCP29A depletion leads to a 50% loss of the *rbcl* transcript under cold conditions. National Center for Biotechnology Information Gene Expression Omnibus (GEO). <https://www.ncbi.nlm.nih.gov/geo/query/acc.cgi?acc=GSE248582>. Deposited 24 November 2023.